FISEVIER

Contents lists available at ScienceDirect

Ceramics International

journal homepage: www.elsevier.com/locate/ceramint





Quasistatic nature of subsurface densification of soda lime silicate glass under nano- and Vickers indentation

Huijing Duan^{a,1}, Andrew L. Ogrinc^{b,1}, Yen-Ting Lin^b, Robert Hengstebeck^c, Bin Dong^d, Jiaxin Yu^a, Slava V. Rotkin^d, Hongtu He^{a,*}, Seong H. Kim^{b,c,**}

- ^a Key Laboratory of Testing Technology for Manufacturing Process, Ministry of Education, Southwest University of Science and Technology, Mianyang, Sichuan, 621010,
- ^b Department of Chemical Engineering, Pennsylvania State University, PA, 16802, USA
- ^c Materials Research Institute, Pennsylvania State University, PA, 16802, USA
- d Department of Engineering Science & Mechanics, Pennsylvania State University, University Park, PA, USA

ARTICLE INFO

Handling Editor: Dr P. Vincenzini

Keywords:
Soda lime silicate glass
Indentation
Densification
Mechanical properties
Sodium ion migration

ABSTRACT

Mechanical properties of glass are critical for technical applications, thus comprehending the material response to mechanical tests is of great importance. In this study, we employ the nanoindentation combined with nanoscale infrared (nano-IR) spectroscopy combined with scattering-type scanning near-field optical microscopy (s-SNOM) and ToF-SIMS, to elucidate the nanoindentation rate dependence of plastic deformation of soda lime silicate glass. Experiment results show that the nanohardness and elastic modulus of soda lime silicate (SLS) glass exhibit a strong dependence on loading rate, while those of fused quartz (FQ) shows a much weaker dependence. The residual indent volume at fast loading conditions is smaller for SLS glass than FQ; but as the loading rate decreases, the residual indent volume of FQ and SLS glass becomes similar. The indent volume of SLS glass after sub-Tg annealing (reverting subsurface densification) shows negligible dependence on the loading rate, suggesting that the densification of SLS glass is strongly enhanced at lower indentation rate, but the shear flow is independent or weakly dependent. Using nanoscale infrared spectroscopy and ToF-SIMS techniques, the sodium ion migration in SLS glass surface in the indent is found to be associated with the subsurface densification. These results suggest the possible role of highly mobile sodium ions on in nano- and micro-scale plastic deformation behavior of SLS glass.

1. Introduction

Silicate glasses are widely used in commercial products such as windows and optics [1], and their applications rely on the surface strength [2]. Thus, the need to better understand mechanical properties of silicate glass is increasing. To that end, indentation tests are widely used to characterize hardness [3], stiffness [4], crack initiation resistance [5], susceptibility to densification [6], and indentation fracture toughness [7]. Nonetheless, the subtlety of the indentation method or data interpretation still needs to be investigated further, which include effects of sample preparation history [8], indenter tip geometry [9], and ambient temperature and humidity [10]. Thus, it is of critical importance to fully comprehend how the glass material responses to

indentation in various test conditions.

When an indenter tip is pressed into the silicate glass surface, the plastic deformation of silicate glass surface can occur, which leaves an imprint (indent) [11]. Generally, two types of plastic deformation can take place during indentation of silicate glass: subsurface densification and isochoric flow [12]. Under the indentation, normal glasses exhibit significant isochoric flow a with small degree of densification, while anomalous glasses exhibit primarily densification with little isochoric flow [13]. Silica and borosilicate are typically considered as anomalous glass, and soda lime silicate (SLS) is considered as a good example of normal glass. But can we really say the degree of subsurface densification is much smaller for SLS than silica based on measurements at a single indentation rate suggested in the ASTM standard [14]?

^{*} Corresponding author.

^{**} Corresponding author. Department of Chemical Engineering, Pennsylvania State University, PA, 16802, USA. *E-mail addresses*: hehongtu@swust.edu.cn (H. He), shk10@psu.edu (S.H. Kim).

¹ The authors contributed equally to the paper.

Many details of the indentation behavior of glass are found to be dependent on the applied load and indenter tip geometry. For instance, the Vickers hardness (*H*v) of silica and SLS glass decreases as the indentation depth increases at higher applied load, which is often called indentation size effect (ISE) [15]. It was believed that the decrease in *H*v was linked to the increase in volume fraction of plastic flow [16]. The increase in indenter sharpness can reduce the magnitude of the ISE and densification, thus lowering the crack initiation resistance of oxide glass [17].

In addition to the applied load and glass composition, the indentation time is also an important factor influencing the plastic deformation of silicate glass. With the increase in holding time, the Young's modulus of hydrated SLS glass decreased due to the water in the glass promoted the viscous flow during the indentation process [18]. With the loading rate increasing from 1 to 1000 mN/s, the nanohardness and elastic modulus of SLS glass was reported to increase by ~ 9 % and ~ 7 %, respectively [19]. In the case of aluminosilicate glass, the nanohardness and elastic modulus were reported to increases by ~ 10.9 % and ~ 2.3 % with an increase of loading rate from 100 to 20,000 μ N/s, respectively [20]. After the Na+-K+ ion exchange treatment for 48 h, the increasement in nanohardness and elastic modulus of aluminosilicate glass was reduced to ~ 8.5 % and ~ 1 % at the same range of loading rate condition, respectively [20]. These findings imply the contact time during the indentation process play an important role in the plastic deformation behaviors of glass.

This work investigated two important questions: (1) How does the indentation rate or time affect the subsurface densification and plastic flow of glass? (2) How is the atomic structure in the subsurface region changed in response to contact stress during the indentation process? To answer these questions, the nanoindentation behavior of SLS glass at different loading rates were systematically analyzed. The corresponding nanohardness and elastic modulus under various loading conditions were compared. The post-indentation and post-annealing imprints were analyzed with atomic force microscopy to determine the degree of subsurface densification and plastic flow. To reveal the contact time dependence of subsurface chemical structure evolution of SLS glass, the nanoscale IR spectroscopy (nano-IR) and the scattering-type scanning near-field optical microscopy (s-SNOM) imaging as well as time-of-flight secondary ion mass spectrometry (ToF-SIMS) imaging of indented area of SLS glass were analyzed. As a reference, the loading rate dependence of nanoindentation behavior of FQ was also studied. The comparison of the SLS glass and FQ data provided an important insight into the role of highly mobile modifier ion (sodium ions) in plastic deformation behavior of SLS glass.

2. Materials and methods

The glass samples used in the present study were SLS float glass (Asahi Glass Company, Tokyo, Japan) with 2 mm thickness and FQ substrate (Corning 7980, Corning, USA) with 1 mm thickness. To avoid the effect of tin [21], only the air-side of the float glass substrates was used in the present study. The nominal bulk composition of the glass substrate by weight% was 72.3 % SiO₂, 13.3 % Na₂O, 7.7 % CaO, 1.9 % Al₂O₃, 4.4 % MgO, 0.3 % K₂O, and 0.1 % Fe₂O₃, as measured with X-ray fluorescence. To remove the surface contamination on the sample surfaces which may affect the experiment results, the glass substrates were ultrasonically cleaned sequentially in acetone and ethanol solutions, and finally rinsed by deionized water before drying with nitrogen gas.

Nanoindentation experiments were performed with a nanoindenter (G200, Agilent Technologies, Inc., Santa Clara, CA) and a three-sided pyramid shape of Berkovich tip with a nominal radius of 200 nm. The normal load was set as 8 mN, and the loading time was set as 5 s, 30 s, and 120 s, which corresponded to a loading rate of 1600 μ N/s, \sim 267 μ N/s, and \sim 67 μ N/s, respectively. Both the holding time and unloading time were 5 s. Based on the typical Oliver-Pharr model [22], the elastic modulus and nanohardness were calculated from unloading curves. The

Poisson's ratio of SLS and FQ was set as 0.23 and 0.17, respectively [23]. All the nanoindentations tests were performed at room temperature (22 \pm 0.3 °C) and room humidity (40 \pm 2 % RH), and each experiment under the given conditions was repeated individually at least 20 times to ensure the reproducibility. To eliminate the effect of thermal drift on nanoindentation, thermal drift correction was reduced to \leq 0.05 nm/s before each test. Vickers indentation tests were performed by a Qness Q60 A+ microindenter (QATM, Mammelzen, Germany) equipped with a four-sided pyramidal diamond Vickers indenter tip. The normal load was set to 0.25 N, which resulted in uniform indents with no cracking at ambient relative humidity (\sim 40 % RH). While the loading time was kept constant, instead the holding time (time the indenter spent at maximum indentation depth) was adjusted to either 10 s, 60 s, or 240 s. The volume and size of the indents was then evaluated using a Zygo NexView 3D Optical Surface Profiler (Zygo Corporation, Middlefield, USA).

After the nanoindentation tests, the residual indentation imprints were scanned by atomic force microscopy (AFM, SPI3800 N, Seiko, Japan) in the tapping mode with a sensitive silicon nitride tip (μ -Masch Technologies, USA). The tip curvature was checked with a reverse-scanning tip topography sample-TGT1 (NT-MDT, Moscow, Russia), and the radius of silicon nitride tip was found to be ~8 nm. The nominal spring constant of silicon nitride tip was 40 N/m. The scan size of all AFM images was 3 \times 3 μ m². To reveal the nanoindentation-induced subsurface damage, both the SLS glass and FQ were annealed at 0.9 \times $T_{\rm g}$ (K) for 3 h and then the nanoindentation marks were re-imaged by AFM. To differentiate the nanoindentation marks before and after annealing treatment, those samples before and after the sub- $T_{\rm g}$ annealing treatment will be referred as 'pristine' and 'annealed', respectively, hereafter.

Nanoscale IR spectroscopy analysis was performed using a custommade neaSNOM microscopy (-neaspec GmbH) equipped with atomic force microscopy (AFM), and combined UV-Vis-NIR-MIR system of pulsed and continuous-wave (CW) laser sources. More details about the nanoscale IR spectroscopy could be found in our previous publication [24]. To obtain background-free nano-FTIR spectra, the AFM of the s-SNOM setup was operated in intermittent contact mode, where the AFM tip was oscillating vertically (\sim 50 nm) with a frequency Ω close to the mechanical resonance frequency of the cantilever. For separating the near-field signal from spurious far-field signal contributions, demodulation of the detector signal at a higher harmonics n of Ω (n > 1) was used. Each sample spectrum was normalized to a reference spectrum measured on a clean silicon sample surface, vielding normalized near-field amplitude and phase spectra, $S_n/S_n(Si)$ and $\varphi_n-\varphi_n$ (Si), respectively. Near-field amplitude and phase spectra with demodulation order n = 2 was plotted. The data was recorded with a spectral resolution of 8 cm⁻¹. For s-SNOM imaging, an 8-chip set of mid-IR tunable quantum cascade lasers (Daylight Solutions) generated MIR CW illumination with wavenumbers ranging from 800 cm⁻¹ and 1400 cm⁻¹. The back-scattered IR amplitude (S_n) and phase (φ_n) signals were recorded in a pseudo-heterodyne detection mode at the second harmonic (n = 2) of the tapping frequency of the AFM probe to extract the near-field signal without background interference. Pt-coated Si AFM tip with an apex radius of ~25 nm (Arrow NCPt, Nanoworld) was used and operated with a tapping amplitude of \sim 50 nm. The scanned area was 3 $\mu m \times 3 \mu m$ for the nanoindentation mark.

ToF-SIMS was conducted with a PHI nanoTOF II instrument. The samples were analyzed with a Bismuth liquid metal ion gun (LMIG) tuned at 30 kV for $\rm Bi^{1+}$. The indented areas were located from a 200 $\mu m \times 200~\mu m$ scan and then the data was collected with a raster of 50 $\mu m \times 50~\mu m$ with $1024~\times~1024$ pixels density. The sample was charge compensated using low energy electrons (<5 eV) and low energy Ar ions (<10 eV) between pulses of the primary ions. Since the micro indents result in a localized change in surface topography, the sodium positive ion signal was normalized to $^{28} \rm Si$ to mitigate this effect. The dynamic SIMS analysis for depth profiling was not performed because the sputtering process would alter the sodium ion distribution [25,26].

3. Results and discussion

3.1. Loading rate dependence of nanomechanical properties

Fig. 1a shows the typical load-displacement curve of SLS and FQ glass measured at three different loading rate conditions. Based on the force-displacement curve in Fig. 1a, the elastic and plastic energy of glass during nanoindentation could be estimated [27]. It is found that as the loading rate increases from 67 to 1600 $\mu N/s$, the elastic energy of SLS glass increases from ${\sim}3.9\times10^{-10}$ J to ${\sim}4.4\times10^{-10}$ J and the plastic energy increases from \sim 4.1 \times 10⁻¹⁰ J to \sim 6.4 \times 10⁻¹⁰ J (Fig. 1b). In the case of FQ, the elastic energy of FQ increases from $\sim\!4.8\times10^{-10}$ J to $\sim\!5$ \times 10⁻¹⁰ J and the plastic energy increases from \sim 2.5 \times 10⁻¹⁰ J to \sim 2.9 \times 10⁻¹⁰ J (Fig. 1c), under the same loading rate range conditions. Clearly, the SLS glass dissipate the indentation energy through both plastic and elastic deformations, while the FQ dissipates more indentation energy through elastic deformation than plastic deformation. While the h_f of FQ seems to be unchanged with loading rate, the h_f of SLS increases when the loading rate is decreased (i.e., longer loading time). Note that the indentation size effect (ISE) or penetration depth dependence can be ruled out. The nanohardness and elastic modulus of SLS glass and FQ as a function of penetration depth are shown in Fig. S1 in Supporting Information. This data suggests that ISE is most significant for indentation depths less than \sim 50 nm for SLS and \sim 30 nm for FQ. In the present study, the maximum penetration depth of SLS glass and FQ is about 250-300 nm, which is far beyond the critical depth of ISE in SLS glass and FO.

The creep distance during the 5 s holding between loading and unloading steps decreases as the loading rate decreases (Fig. 1b). This means that when the indentation rate is fast, the plastic deformation could not occur to its full capacity and additional deformation (either densification or isochoric flow) takes place even though the applied load is kept constant. Overall, the creep distance of SLS glass is slightly higher than FQ under the same loading conditions. This could be related to the displacement and reorganization of sodium modifier ions in the SLS glass network [13].

The unloading part of the load-depth curve in Fig. 1a was processed with the standard Oliver-Pharr model [28] to quantify the dependence of nanohardness and elastic modulus of SLS glass and FQ changing on loading rate. The results are shown in Fig. 2. As the loading rate decreases by $\sim\!24$ times (from 1600 µN/s to $\sim\!67$ µN/s), the nanohardness and elastic modulus of SLS glass decreases by $\sim\!15$ % (from $\sim\!6.66$ to $\sim\!5.67$ GPa) and $\sim\!6.4$ % (from $\sim\!79.3$ GPa to $\sim\!74.2$ GPa), respectively. For the same change in the loading rate, FQ shows a much smaller decrease in nanohardness ($\sim\!0.5$ %) and elastic modulus ($\sim\!2.5$ %). The most significant change occurred between $\sim\!267$ µN/s and $\sim\!67$ µN/s, which corresponds to an average penetration rate of $\sim\!9$ nm/s to $\sim\!2$ nm/s (ignoring the nonlinearity seen in Fig. 1a).

The plastic deformation of FQ during the indentation is mostly through subsurface densification [3,13]. So, very little dependence of nanohardness and elastic modulus means that the rate of subsurface densification of FQ is faster than the probe rate used in this study (1600 $\mu N/s$ loading rate, which corresponds to $\sim\!53$ nm/s in penetration rate). In contrast, SLS can dissipate the indentation energy through both subsurface densification and isochoric flow. Thus, we hypothesized that the indentation rate dependence of SLS – more plastic deformation and less creep at lower indentation rate (i.e., longer indentation time) – is due to a change in the relative extent of these two competing processes during the indentation. To test this hypothesis, we measured the volume recovery upon annealing of nanoindented surfaces and determined the percentage of densification and isochoric flow at a given indentation rate.

3.2. Loading rate dependence of plastic deformation

Fig. 3a compares the cross-section line profile of residual nano-indentation imprints on SLS glass surface. There is slightly pile-up around the periphery of pristine nanoindentation of SLS glass (Fig. 3a). Since the pile-up is small, it had a negligible impact on the nanohardness and elastic modulus of SLS glass using the Oliver-Pharr model [29]. The residual depth of nanoindentation of SLS glass is found to significantly increase as the loading rate is changed from ~ 267

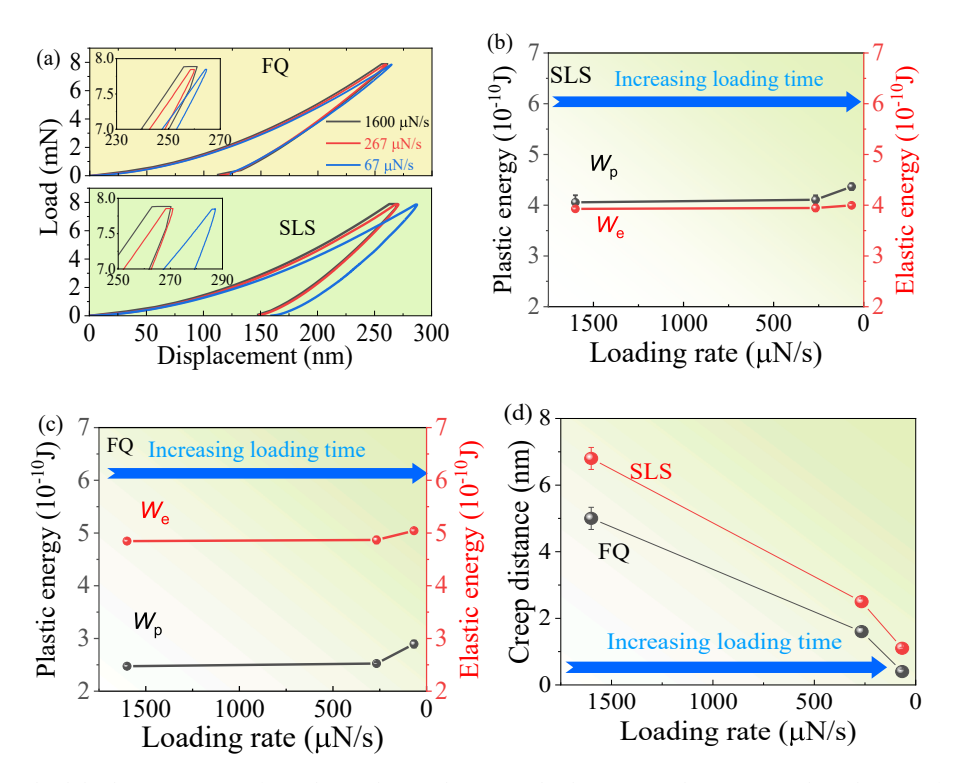


Fig. 1. (a) Nanoindentation load-displacement curve of SLS glass and FQ under various loading rate conditions. Insets show the magnified load-displacement curve at the maximum load-displacement curve regime. (b) Creep distance of SLS glass and FQ under various loading rate conditions.

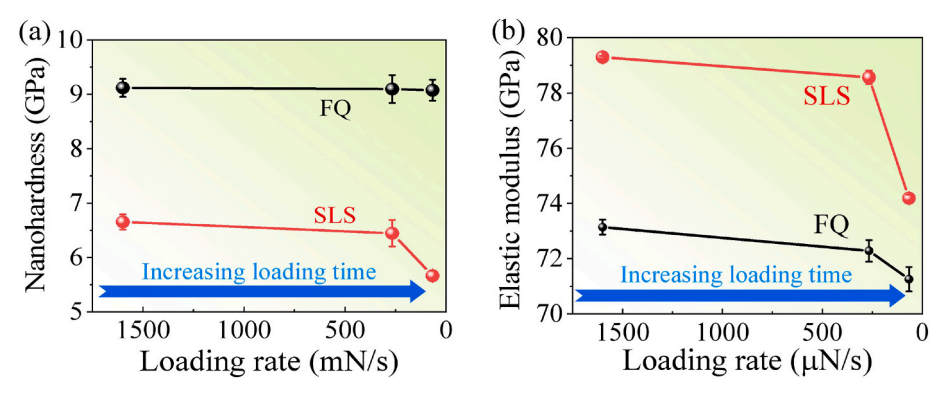


Fig. 2. (a) Nanohardness and (b) elastic modulus of SLS glass and FQ under various loading rate conditions.

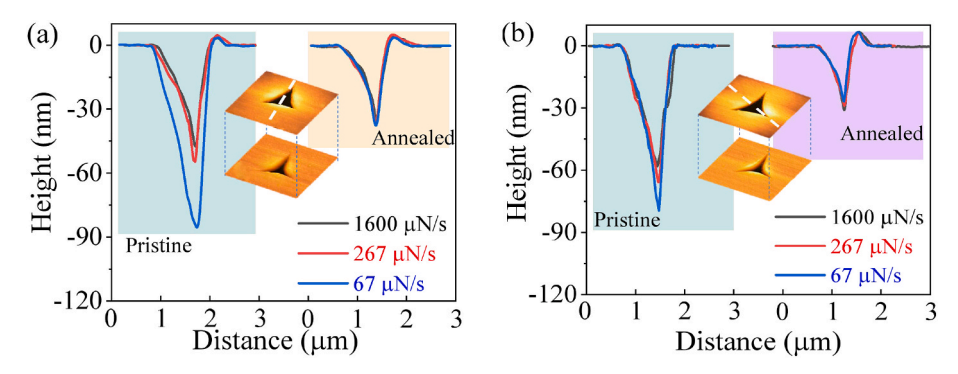


Fig. 3. Cross-section line profile of pristine nanoindentation and annealed nanoindentation of (a) SLS glass and (b) FQ under various loading rate conditions. Inset images show the corresponding typical AFM images of pristine (up) and annealed (down) nanoindentation. The white dotted lines show the position where the cross-section line profiles are taken.

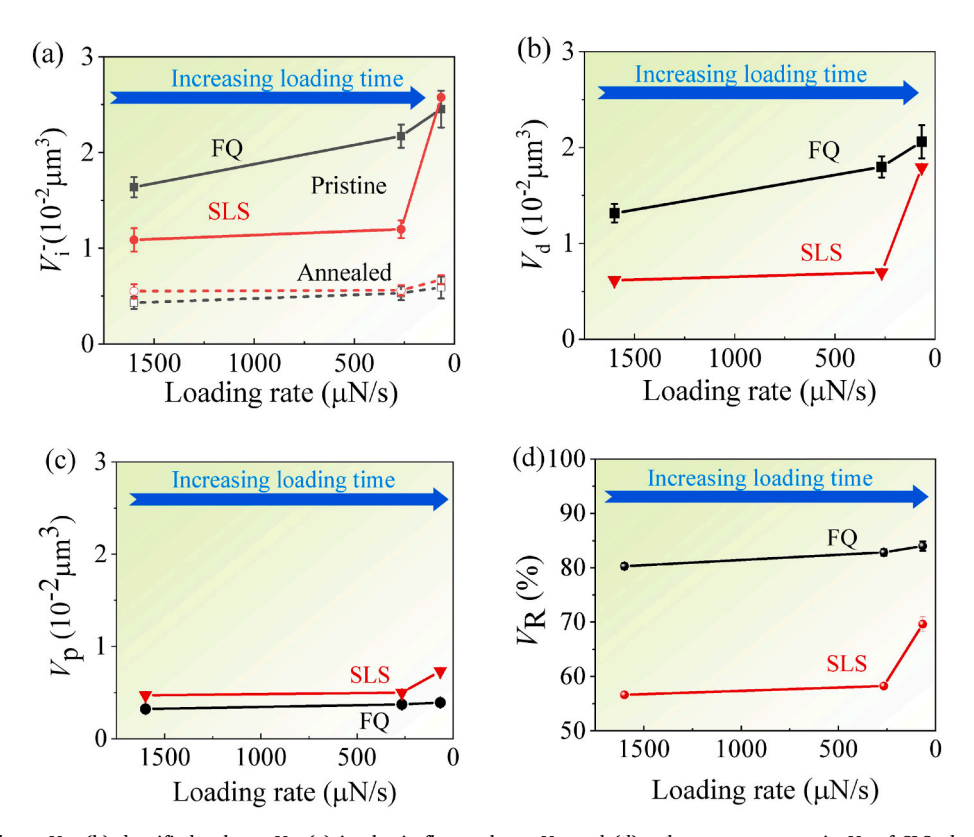


Fig. 4. (a) Indented volume V_i^- , (b) densified volume V_d , (c) isochoric flow volume V_p , and (d) volume recovery ratio V_R of SLS glass and FQ under various nanoindentation loading rate conditions.

 $\mu N/m$ to ${\sim}67~\mu N/s$, while only a marginal increase is observed when the loading rate is changed from 1600 $\mu N/s$ to ${\sim}267~\mu N/s$. This is consistent with the trend seen in the nanohardness data in Fig. 3a. In contrast, there is no pile-up around the periphery of pristine nanoindentation of FQ surface and the residual depth of the nanoindentation shows a weaker loading rate dependence (Fig. 3b).

Fig. 4a compares the residual indentation volume (V_i^-) of SLS and FQ glasses after nanoindentation at three different loading rates. As the loading rate is decreased from 1600 µN/s (\approx 53 nm/s penetration rate) to 267 µN/s (\approx 9 nm/s), the V_i^- of SLS glass does not change much (from \sim 1.1 \times 10⁻² µm³ to \sim 1.2 \times 10⁻² µm³); but then as the rate is decreased from 267 µN/s to 67 µN/s (\approx 2 nm/s), it increases significantly from \sim 1.1 \times 10⁻² µm³ to \sim 2.57 \times 10⁻² µm³. In contrast, the V_i^- of FQ is \sim 1.64 \times 10⁻² µm³ at the highest loading rate used and gradually increases to \sim 2.45 \times 10⁻² µm³ at the lowest loading rate. It is intriguing to note that although the elastic-plastic deformation mechanisms of SLS and FQ glass are quite different [3,13], the residual volume becomes comparable when the loading rate is sufficiently low enough.

To quantitatively compare the subsurface densification and plastic flow, the nanoindentation volume change before and after sub- $T_{\rm g}$ annealing are measured following the methods by Yoshida et al. [30, 31]. The line-profiles of the annealed nanoindentation are compared with those of the pristine nanoindentation in Fig. 3, from which the densified volume ($V_{\rm d}$), plastic flow volume ($V_{\rm p}$), and volume recovery ratio ($V_{\rm R}$) were calculated [30,31].

As the loading rate is decreased, the V_d of SLS increases from 0.61 \times $10^{-2}~\mu\text{m}^3$ at 1600 $\mu\text{N/s}$, marginally to \sim 0.70 \times $10^{-2}~\mu\text{m}^3$ at \sim 267 $\mu\text{N/s}$, and suddenly to \sim 1.8 \times $10^{-2}~\mu\text{m}^3$ at \sim 67 $\mu\text{N/s}$. Meanwhile, the V_p of SLS remains relatively constant at \sim 0.5 \times $10^{-2}~\mu\text{m}^3$ when the

indentation rate is equal to or lower than ~267 $\mu N/s$, and marginally increases to ~0.73 \times 10^{-2} μm^3 at the ~67 $\mu N/s$ rate. This leads to only marginal change in V_R within the 57–58 % at the indentation rate below ~267 $\mu N/s$ and a sudden increase to ~70 % at the ~67 $\mu N/s$ rate. In contrast, the V_R and V_P of FQ remained relatively constant in the 80–84 % and 0.32–0.39 \times 10^{-2} μm^3 , respectively, while the indentation rate changed by ~25 times (Fig. 4). Moreover, when the environment humidity is decreased to 10 %, similar V_R dependence on the loading rate of SLS glass and FQ could be found (Fig. S2 in Supporting Information).

FQ consists of the amorphous network of Q^4 species only, so it has a relatively large free volume in the network [13]. In contrast, the SLS glass has a distribution of Q^2 , Q^3 and Q^4 species and the space between Si–O–Si networks is occupied by modifier ions (sodium and calcium ions); thus, SLS has much less free volume than FQ [13]. When the FQ surface is compressed by an indenter, the network in the subsurface region can easily be densified because it has a large free volume. In the case of SLS with much less free volume, its network is less prone to densification and more prone to isochoric flow (thus, V_R is much lower than FQ).

However, this simple picture cannot explain the indentation rate dependence of the $V_{\rm R}$ of SLS glass, especially the sudden increase at a very low indentation rate (Fig. 4d). It must mean the occurrence of a secondary densification process which takes place very slowly. It is speculated that it might be due to the migration of sodium ions under the applied stress gradient [32,33]. Such a process is expected to be slow at room temperature. The diffusion of sodium ions from the high stress region to the lower stress region may occur, which may be accompanied with structural rearrangement of the glass network since there is no other cationic species that can diffuse into the high stress region to

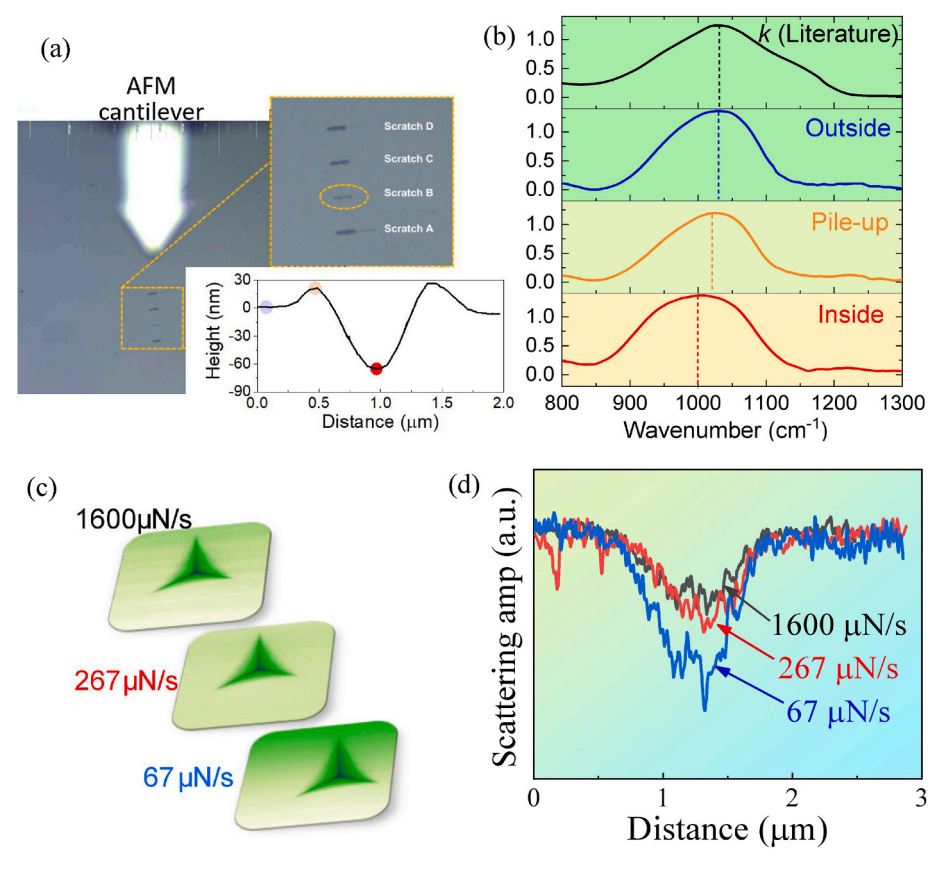


Fig. 5. (a) Optical image of nanoscratch lines made with a cono-spherical tip at a constant load of 7 mN SLS glass and cross-sectional line profile of one of the scratch lines. (b) Imaginary part (k) of complex refractive index (n+ik) calculated from the measured amplitude (S_2) and phase (φ_2) of the nano-FTIR signals at the pristine surface (blue dot position) versus the pile-up (orange) and valley (red) of the nanoscratch track. (c) S_2 -intensity map at 980 cm⁻¹ obtained over a 3 μm × 3 μm area of nanoindentation made with Berkovich tip on SLS at three loading rates. (d) Cross-sectional line profiles of the S_2 images shown in (c). (For interpretation of the references to colour in this figure legend, the reader is referred to the Web version of this article.)

compensate the remaining Si-O nonbridging oxygen species.

3.3. Contact time enhanced sodium ion migration at SLS glass surfaces

Based on the amplitude (S_2) and phase (φ_2) spectra of the near-field scattered IR signals, the local optical constant (complex refractive index, n+ik) of the surface can be obtained, which can be related to the glass network structure in the subsurface region [24]. Fig. 5a shows the optical image and line profiles of nanoscratch lines made on SLS glass and Fig. 5b displays the k-spectra of complex refractive index (which is equivalent to IR absorption spectra in the Si–O stretching vibration region) measured at the outside (reference) region and at the pile-up and valley regions of nanoscratch line. The details of calculating the optical constant spectra from the scattered IR spectra are shown in the Supporting Information. The peak shape of the k-spectrum of the outside region is somewhat different from the literature spectrum due to some assumptions made in the signal conversion [24], but the peak position with the maximum intensity outside the nanoscratch region is in good agreement with the literature [21].

The peak position of the Si–O stretch band in the *k*-spectra of the pileup and valley regions of the nanoscratch shows a red-shift as compared to that of the outside reference region (Fig. 5b). This red-shift can be interpreted as an elongation of the Si–O bond length which should be accompanied by an increase in the Si–O–Si bond angle [34,35]. The decrease in the Si–O–Si bond angle is directly related to the densification process of silica glass [3,13,24]. We speculate that the same is relevant to the silicate glass network.

Fig. 5c displays the 980 cm⁻¹ S_2 -amplitude maps of the nanoindentation made with the Berkovich tips at three different loading rates and the corresponding cross-sectional intensity profiles are shown in Fig. 5d. This wavenumber was chosen for S_2 amplitude mapping since it represents the characteristic of densified region (980 cm⁻¹ in S_2 amplitude, 1000 cm⁻¹ in calculated k spectra) and gives a large contrast between the pristine region and the densified region in the scattering amplitude raw signal (see Figs. S2–S4 in Supporting Information). It is clearly seen that the 980 cm $^{-1}$ scattering intensity inside the nanoimprint becomes smaller at the slower loading rate, which is interpreted as more degree of subsurface densification. This result is in good agreement with the trend found from the sub- T_g annealing experiment (Fig. 4d).

Note that the S_2 -amplitude at 980 cm⁻¹ in the s-SNOM IR analysis should not be directly compared with the peak position in the k-spectrum and cannot be interpreted in terms of changes in the NBO stretch mode in silicate glass [36–39]. In fact, the 980 cm⁻¹ shoulder in the specular reflection IR spectrum of SLS cannot be interpreted as the local vibrational mode of the Si–O (NBO) bond [40,41].

In addition to the changes in the bond length and angle distributions of the Si–O–Si network, the modifier ions migration can also occur under an applied stress [33]. The most likely ions to move in SLS glass under a stress gradient is sodium ions. ToF-SIMS imaging was used to quantify the extent of sodium migration inside the nanoindentation. Due to limitations in the spatial resolution of the instrument, the migration was quantified on Vickers indents of SLS with variable holding time, instead of loading time. However, this should still enable investigation of the importance of sodium migration with indents which have different loading-time behavior. When the Vickers indentation was done on SLS glass surfaces with three different holding times (10 s, 60 s, 240 s at 0.25 N applied load), the volume recovery ratio (Fig. 6b) of SLS glass increases, which is qualitatively consistent with the trend found in the nanoindentation with varying indentation rates (Fig. 4d).

Fig. 6c displays the ToF-SIMS mapping of the Na signal (normalized to the Si signal) around the Vickers indent imprints made with three different holding times, with the corresponding cross-sectional intensity profiles are shown in Fig. 6d. The ToF-SIMS analysis found that the Na/Si ratio is noticeably higher inside the indented region than the outside region. This finding implies that as the glass is indented, sodium ions in

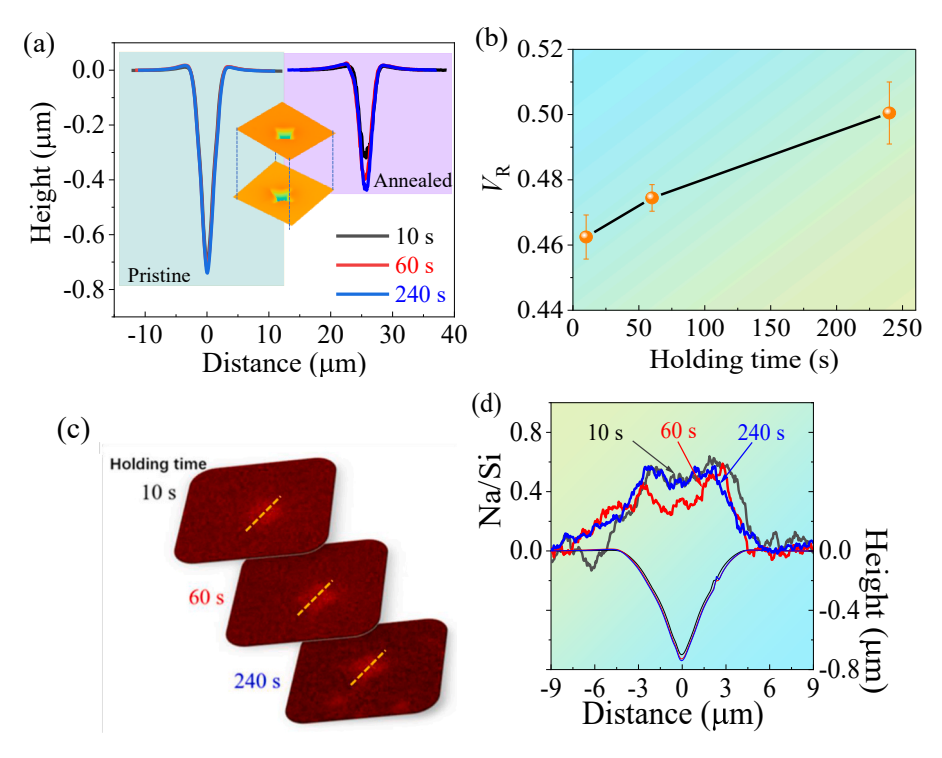


Fig. 6. (a) Cross sectional line profiles of pristine and annealed Vickers indentation on SLS glass made with three different holding times at the 0.25 N applied load. (b) Volume recovery ratio (V_R) of Vickers indent after sub- T_g annealing treatment. (c) ToF-SIMS image of sodium ion distribution (normalized to the Si signal) around the Vickers indent on SLS glass surface made with three different holding times. The dotted lines show the position where the line profile of the Na/Si ToF-SIMS image are taken. (d) Vertical direction line profiles of the Na/Si ToF-SIMS image shown in (c). The tip used in Vickers indentation is a four-sided pyramidal diamond Vickers indenter tip.

the near-surface region in contact with the indenter tip migrate to the glass surface (within the depth probed by static SIMS). This process may be coupled with the previously discussed changes in the bond length and bond angle which occurs during plastic deformation of the glass.

The migration of sodium to the SLS surface is believed to be caused by the subsurface densification. The densification of the silicate network in the subsurface region of the glass, and the accompanying structural changes, may drive the mobile sodium ions towards the surface. Another explanation is that the sodium enhancement is due to frictional shear between the indenter tip and the glass surface. The presence of pile-up in the periphery of the indent (Fig. 6a) indicates that some isochoric shear flow has occurred, and it is known that frictional damage can cause a drastic change in the chemistry of the topmost surface [42,43]. At this moment, it is not possible to differentiate these effects and determine which is the more dominant factor. While this behavior is interesting and warrants future study, it cannot fully explain the increase in densification volume (Fig. 4b) because the amount of sodium detected with ToF-SIMS at the topmost surface did not vary with the holding time (Fig. 6d). When the sodium ion is migrated to the surface during the indentation process, the remained subsurface region will become silica-rich. Since the silica-rich structure has more propensity to be densified, the degree of sodium ion migration may affect the $V_{\rm R}$ of SLS glass. However, the amount of sodium ion detected with ToF-SIMS at the topmost surface did not vary with the holding time (Fig. 6d) and we do not know the exact stoichiometry from ToF-SIMS. Thus, more studies are needed to reveal the relationship between the sodium ion migration at SLS glass surface and V_R during indentation process in the future.

If sodium ions can be pushed to the glass surface during the indentation, it is also likely that they are displaced laterally along the stress gradient. It was reported that a gradient of hydrostatic pressure can drive the mobile sodium ions from the compressed region to the tensile region [44]. The mobility of sodium ions in silicate glass has also been reported under compressive stress [45], tensile stress [32,33], and frictional stress [32]. The same effect may occur in the stress gradient region around the indenter during nanoindentation. Such migrations may be exaggerated when plastic deformation occurs.

The findings of this work add more degrees of freedom to future indentation studies. The extent of subsurface densification during indentation will be functions not only of glass composition [13], indenter tip geometry [17,31], and indentation load [13], but also indentation loading rate [19,20] and holding time [46]. It is also possible that the migration of modifier ions to the surface and/or laterally away from the compressed region impact the indentation behavior [32,33,44,45]. In addition, the plastic deformation of the subsurface region is a function of humidity outside the glass because it affects the friction at the indenter/glass interface during the tip penetration [21,39,43,45,47,48]. The comparison of indentation hardness among different glasses should be made by considering not only the glass composition, but also these extrinsic factors.

4. Conclusions

Nanoindentation, nano-IR, and ToF-SIMS analyses were employed to elucidate the loading rate dependence of plastic deformation of SLS glass. It was found that the nanohardness and elastic modulus of SLS glass shows a strong dependence on loading rate, while those of FQ shows a weak dependence. The subsurface densification of SLS is enhanced at a slower indentation rate, but the shear flow is not affected much. The subsurface densification appears to be coupled with the so-dium ion migration at the surface of SLS as well as changes in the silicate network structure.

CRediT authorship contribution statement

Huijing Duan: Writing – review & editing, Writing – original draft, Software, Methodology, Investigation, Formal analysis, Data curation.

Andrew L. Ogrinc: Writing – review & editing, Writing – original draft, Software, Methodology, Investigation, Formal analysis, Data curation. Yen-Ting Lin: Writing – review & editing, Investigation, Data curation. Robert Hengstebeck: Writing – review & editing, Investigation, Data curation. Bin Dong: Writing – review & editing, Investigation, Data curation. Jiaxin Yu: Writing – review & editing, Funding acquisition. Slava V. Rotkin: Writing – review & editing, Software. Hongtu He: Writing – review & editing, Writing – original draft, Validation, Supervision, Software, Resources, Methodology, Investigation, Funding acquisition, Formal analysis, Data curation. Seong H. Kim: Writing – review & editing, Validation, Supervision, Resources, Methodology, Investigation, Funding acquisition, Formal analysis, Data curation.

Declaration of competing interest

The authors declare that they have no known competing financial interests or personal relationships that could have appeared to influence the work reported in this paper.

Acknowledgements

This work is supported by National Natural Science Foundation of China (Grant No. 51975492) and the funding from Sichuan Provincial Department of Science and Technology (24NSFSC0147 and 24NSFTD0019), and the ToF-SIMS and s-SNOM analyses were conducted with the support from the National Science Foundation (Grant No. DMR-2011410). The co-authors acknowledge the Penn State Materials Characterization Lab for use of the PHI nanoTOF II, Qness Q60 A+ microindenter, and the Zygo NexView 3D Optical Surface Profiler.

Appendix A. Supplementary data

Supplementary data to this article can be found online at https://doi.org/10.1016/j.ceramint.2024.06.054.

References

- H. Li, K. Wu, J. Lim, H. Song, V.I. Klimov, Doctor-blade deposition of quantum dots onto standard window glass for low-loss large-area luminescent solar concentrators, Nat. Energy 1 (2016) 16157, https://doi.org/10.1038/ nenergy.2016.157.
- [2] C. Liu, Y. Ji, J. Tang, K. Otsuka, Y. Wang, M. Hou, Y. Hao, S. Ren, P. Luo, T. Ma, D. Wang, X. Ren, A lightweight strain glass alloy showing nearly temperature-independent low modulus and high strength, Nat. Mater. 21 (2022) 1003–1007, https://doi.org/10.1038/s41563-022-01298-y.
- [3] T. Rouxel, J. Jang, U. Ramamurty, Indentation of glasses, Prog. Mater. Sci. 121 (2021) 100834, https://doi.org/10.1016/j.pmatsci.2021.100834.
- [4] T. Rouxel, J. Jang, U. Ramamurty, Indentation of glasses, Prog. Mater. Sci. 121 (2021) 100834, https://doi.org/10.1038/s41563-020-0684-x.
- [5] G.N. Greaves, A.L. Greer, R.S. Lakes, T. Rouxel, Poisson's ratio and modern materials, Nat. Mater. 10 (2011) 823–837, https://doi.org/10.1038/nmat3134.
- [6] L. Wondraczek, E. Bouchbinder, A. Ehrlicher, J.C. Mauro, R. Sajzew, M. M. Smedskjaer, Advancing the mechanical performance of glasses: perspectives and challenges, Adv. Mater. 34 (14) (2022) 2109029, https://doi.org/10.1002/ adma.202109029.
- [7] A.J.D. Shaikeea, H. Cui, M. O'Masta, X.R. Zheng, V.S. Deshpande, The toughness of mechanical metamaterials, Nat. Mater. 21 (2022) 297–304, https://doi.org/ 10.1038/s41563-021-01182-1.
- [8] K. Gall, K. Juntunen, H.J. Maier, H. Sehitoglu, Y.I. Chumlyakov, Instrumented micro-indentation of NiTi shape-memory alloys, Acta Mater. 49 (16) (2001) 3205–3217, https://doi.org/10.1016/S1359-6454(01)00223-3.
- [9] H. Bei, E.P. George, J.L. Hay, G.M. Pharr, Influence of indenter tip geometry on elastic deformation during nanoindentation, Phys. Rev. Lett. 95 (2005) 045501, https://doi.org/10.1103/PhysRevLett.95.045501.
- [10] N.D. Surdyka, C.G. Pantano, S.H. Kim, Environmental effects on initiation and propagation of surface defects on silicate glasses: scratch and fracture toughness study, Appl. Phys. A 116 (2014) 519–528.
- [11] V. Keryvin, L. Charleux, R. Hin, J.-P. Guin, J.-C. Sangleboeuf, Mechanical behaviour of fully densified silica glass under Vickers indentation, Acta Mater. 129 (2017) 492–499, https://doi.org/10.1016/j.actamat.2017.03.008.
- [12] E. Barthel, V. Keryvin, G. Rosales-Sosa, G. Kermouche, Indentation cracking in silicate glasses is directed by shear flow, not by densification, Acta Mater. 194 (2020) 473–481, https://doi.org/10.1016/j.actamat.2020.05.011.

- [13] K. Januchta, M.M. Smedskjaer, Indentation deformation in oxide glasses: Quantification, structural changes, and relation to cracking, J. Non-Cryst. Solids X 1 (2019) 100007, https://doi.org/10.1016/j.nocx.2018.100007.
- [14] E. Broitman, Indentation hardness measurements at macro-, micro-, and nanoscale: a critical overview, Tribol. Lett. 65 (2017) 23, https://doi.org/10.1007/s11249-016-0805-5
- [15] A.L. Fry, A.L. Ogrinc, S.H. Kim, J.C. Mauro, Field strength effect on elastoplastic behavior of aluminoborosilicate glass; II. Volumetric recovery, J. Am. Ceram. Soc. 106 (9) (2023) 5213–5232, https://doi.org/10.1111/jace.19152.
- [16] M. Kazembeyki, M. Bauchy, C.G. Hoover, New insights into the indentation size effect in silicate glasses, J. Non-Cryst. Solids 521 (2019) 119494, https://doi.org. 10.1016/j.jnoncrysol.2019.119494.
- [17] J.F.S. Christensen, N.M. Anoop Krishnan, M. Bauchy, M.M. Smedskjaer, Indenting glasses with indenters of varying stiffness and sharpness, J. Non-Cryst. Solids 603 (2023) 122111, https://doi.org/10.1016/j.jnoncrysol.2022.122111.
- [18] N.M. Keulen, Indentation creep of hydrated soda-lime silicate glass determined by nanoindentation, J. Am. Ceram. Soc. 76 (4) (1993) 904–912, https://doi.org/ 10.1111/j.1151-2916.1993.tb05314.x.
- [19] R. Chakraborty, A. Dey, A.K. Mukhopadhyay, Loading rate effect on nanohardness of soda-lime-silica glass, Metall. Mater. Trans. A 41 (2010) 1301–1312, https://doi. org/10.1007/s11661-010-0176-8
- [20] X. Li, L. Jiang, J. Li, I. Mohagheghian, J.P. Dear, L. Li, Y. Yan, Elastic-plastic deformation in ion-exchanged aluminosilicate glass by loading rate dependent nanoindentation, J. Non-Cryst. Solids 491 (2018) 79–88, https://doi.org/10.1016/ iinnervsol.2018.04.003
- [21] H. He, H. Liu, Y. Lin, C. Qu, J. Yu, S.H. Kim, Differences in indentation and wear behaviors between the two sides of thermally tempered soda lime silica glass, J. Am. Ceram. Soc. 104 (9) (2021) 4718–4727, https://doi.org/10.1111/ iace 17872
- [22] W.C. Oliver, G.M. Pharr, An improved technique for determining hardness and elastic modulus using load and displacement sensing indentation experiments, J. Mater. Res. 7 (6) (1992) 1564–1583, https://doi.org/10.1557/JMR.1992.1564.
- [23] O. Goodman, B. Derby, The mechanical properties of float glass surfaces measured by nanoindentation and acoustic microscopy, Acta Mater. 59 (4) (2011) 1790–1799, https://doi.org/10.1016/j.actamat.2010.11.045.
- [24] H. He, Z. Chen, Y.T. Lin, S.H. Hahn, J. Yu, A.C.T. Van Duin, S.H. Kim, T.D. Gokus, S.V. Rotkin, S.H. Kim, Subsurface structural change of silica upon nanoscale physical contact: chemical plasticity beyond topographic elasticity, Acta Mater. 208 (2021) 116694. https://doi.org/10.1016/j.actamat.2021.116694.
- [25] B.M.J. Smets, T.P.A. Lommen, Ion beam effects on glass surfaces, J. Am. Ceram. Soc. 65 (1982) c80–c81, https://doi.org/10.1111/j.1151-2916.1982.tb10453.x.
- [26] Y. Yamamoto, N. Shimodaira, SIMS depth profile analysis of sodium in silicon dioxide, Appl. Surf. Sci. 255 (4) (2008) 860–862, https://doi.org/10.1016/j. apsusc.2008.05.069.
- [27] X. Sun, L. Li, Y. Guo, H. Zhao, S. Zhang, Y. Yu, D. Wu, H. Liu, M. Yu, D. Shi, Z. Liu, M. Zhou, L. Ren, L. Fu, Influences of organic component on mechanical property of cortical bone with different water content by nanoindentation, AIP Adv. 8 (2018) 035003, https://doi.org/10.1063/1.5017807.
- [28] G.M. Pharr, W.C. Oliver, Measurement of thin film mechanical properties using nanoindentation, MRS Bull. 17 (7) (1992) 28–33, https://doi.org/10.1557/ S0883769400041634.
- [29] W.C. Oliver, G.M. Pharr, Measurement of hardness and elastic modulus by instrumented indentation: Advances in understanding and refinements to methodology, J. Mater. Res. 19 (1) (2004) 3–20, https://doi.org/10.1557/ imv.2004.10.13
- [30] S. Yoshida, J.-C. Sanglebœuf, T. Rouxel, Quantitative evaluation of indentationinduced densification in glass, J. Mate. Res. 20 (12) (2005) 3404–3412, https:// doi.org/10.1557/jmr.2005.0418.
- [31] S. Yoshida, H. Sawasato, T. Sugawara, Y. Miura, J. Matsuoka, Effects of indenter geometry on indentation-induced densification of soda-lime glass, J. Mater. Res. 25 (11) (2010) 2203–2211, https://doi.org/10.1557/jmr.2010.0287.

- [32] Y.N. Ahn, J.T. Harris, The effect of individual elements of alkali aluminosilicate glass on scratch characteristics: a molecular dynamics study, J. Non-Cryst. Solids 536 (2020) 119840, https://doi.org/10.1016/j.jnoncrysol.2019.119840.
- [33] F. Célarié, M. Ciccotti, C. Marlière, Stress-enhanced ion diffusion at the vicinity of a crack tip as evidenced by atomic force microscopy in silicate glasses, J. Non-Cryst. Solids 353 (1) (2007) 51–68, https://doi.org/10.1016/j.jnoncrysol.2006.09.034.
- [34] H.S. Liu, S.H. Hahn, M.G. Ren, M. Thiruvillamalai, T.M. Gross, J.C. Du, A.C.T. van Duin, S.H. Kim, Searching for correlations between vibrational spectral features and structural parameters of silicate glass network, J. Am. Ceram. Soc. 103 (2020) 3575–3589, https://doi.org/10.1111/jace.17036.
- [35] H. Liu, H. Kaya, Y.-T. Lin, A. Ogrinc, S.H. Kim, Vibrational spectroscopy analysis of silica and silicate glass networks, J. Am. Ceram. Soc. 105 (4) (2022) 2355–2384, https://doi.org/10.1111/jace.18206.
- [36] J. Luo, H. He, N.J. Podraza, L. Qian, C.G. Pantano, S.H. Kim, J. Mauro, Thermal poling of soda-lime silica glass with nonblocking electrodes-part 1: effects of sodium ion migration and water ingress on glass surface structure, J. Am. Ceram. Soc. 99 (2016) 1221–1230, https://doi.org/10.1111/jace.14081.
- [37] N. Sheth, J. Luo, J. Banerjee, C.G. Pantano, S.H. Kim, Characterization of surface structures of dealkalized soda lime silica glass using X-ray photoelectron, specular reflection infrared, attenuated total reflection infrared and sum frequency generation spectroscopies, J. Non-Cryst. Solids 474 (2017) 24–31, https://doi.org/ 10.1016/j.jnorcrysol.2017.08.009.
- [38] D.M. Sanders, W.B. Person, L.L. Hench, Quantitative analysis of glass structure with the use of infrared reflection spectra, Appl. Spectrosc. 28 (1974) 247–255. htt ps://opg.optica.org/as/abstract.cfm?URI=as-28-3-247.
- [39] J.W. Luo, H. Huynh, C.G. Pantano, S.H. Kim, Hydrothermal reactions of soda lime silica glass - revealing subsurface damage and alteration of mechanical properties and chemical structure of glass surfaces, J. Non-Cryst. Solids 452 (2016) 93–101, https://doi.org/10.1016/j.jnoncrysol.2016.08.021.
- [40] A.L. Ogrinc, Y. Zhou, S.H. Hahn, Y.T. Lin, S.H. Kim, Revealing the structure of the sodium-leached layer of soda lime silica glass: a comprehensive spectroscopic analysis, J. Non-Cryst. Solids 600 (2023) 121989, https://doi.org/10.1016/j. inoncrysol.2022.121989.
- [41] R.D. Shannon, Revised effective ionic radii and systematic studies of interatomic distances in halides and chalcogenides, Acta Crystallogr. Sect. A. 32 (1976) 751–767, https://doi.org/10.1107/S0567739476001551.
- [42] Y.T. Lin, A.L. Ogrinc, A.N. Zoba, J. Lee, S. Jang, N.J. Smith, J. Banerjee, A. Antony, G. Agnello, S.H. Kim, Revealing 'invisible' subsurface structural change/damage in silicate glass made by 'nearly-elastic contact' with a spherical smooth surface, Acta Mater. 264 (2024) 119571, https://doi.org/10.1016/j.actamat.2023.119571.
- [43] S.H. Hahn, H. Liu, S.H. Kim, A.C.T. van Duin, Atomistic understanding of surface wear process of sodium silicate glass in dry versus humid environments, J. Am. Ceram. Soc. 103 (5) (2020) 3060–3069, https://doi.org/10.1111/jace.17008.
- [44] N. Weber, M. Goldstein, Stress-induced migration and partial molar volume of sodium ions in glass, J. Chem. Phys. 41 (1964) 2898–2901, https://doi.org/ 10.1063/1.1263232
- [45] H. Liu, H. He, Z. Chen, S.H. Kim, Flexural stress effect on mechanical and mechanochemical properties of soda lime silicate glass surface, J. Am. Ceram. Soc. 105 (4) (2022) 2847–2857, https://doi.org/10.1111/jace.18250.
- [46] Y. Lai, J. Yu, L. Sun, F. Wang, Q. Zheng, H. He, Nanoindentation creep dependent deformation process of silica and soda lime silicate glass, J. Non-Cryst. Solids 597 (2022) 121906, https://doi.org/10.1016/j.inoncrysol.2022.121906.
- [47] H. He, S.H. Hahn, J. Yu, Q. Qiao, A.C.T. Van Duin, S.H. Kim, Friction-induced subsurface densification of glass at contact stress far below indentation damage threshold, Acta Mater. 189 (2020) 166–173, https://doi.org/10.1016/j. actamat.2020.03.005.
- [48] H. He, Q. Qiao, T. Xiao, J. Yu, S.H. Kim, Effect of humidity on friction, wear, and plastic deformation during nanoscratch of soda lime silica glass, J. Am. Ceram. Soc. 105 (2) (2022) 1367–1374, https://doi.org/10.1111/jace.18147.